Controlling magnetic interfaces using ordered surface alloys

Chenlu Ji,[1] Zhe Wang,[2] Qiang Wu,[1] Li Huang,[2,*] and M. S. Altman[1,†]
[1]*Department of Physics, Hong Kong University of Science and Technology, Clear Water Bay, Kowloon, Hong Kong SAR, China*
[2]*Department of Physics, South University of Science and Technology of China, Shenzhen, Guangdong 518055, China*
(Received 31 July 2016; published 24 October 2016)

We have investigated the growth and magnetic properties of Fe thin films on the clean W(100) surface and W(100)-M $c(2 \times 2)$ (M = Cu, Ag, Au) surface alloy substrates. The influence of the interface on magnetism is assessed experimentally by studying sensitive threshold behavior in magnetic ordering using spin-polarized low-energy electron microscopy. The onset of ferromagnetic order that occurs with increasing film thickness at room temperature due to finite-sized scaling of the Curie temperature varies reproducibly among films on W(100) and the surface alloys. Magnetic moments and exchange coupling constants of the magnetic ground states are also determined theoretically for films with ideal interfaces by first-principles density functional theory calculations. These microscopic quantities are consistently enhanced in Fe films on the noble metal-induced surface alloys compared to their values in films on the clean W(100) surface. We attribute the systematic variation of magnetic onset observed experimentally to the competition between the intrinsically enhanced magnetic coupling and moments on the surface alloy substrates and several extrinsic factors that could suppress magnetic ordering, including intermixing, substrate and film roughness, and surface alloy disorder. Tendencies for intermixing are explored theoretically by determining the energy barrier for noble metal segregation. Despite these possible extrinsic effects, the results suggest that the use of the broad class of ordered surface alloys as alternative substrates may offer greater opportunities for manipulating thin film magnetism.

DOI: 10.1103/PhysRevB.94.134425

I. INTRODUCTION

Magnetic nanostructures have attracted sustained interest for many years because they exhibit a wide range of fascinating and useful physical phenomena, such as low-dimensional magnetism, oscillatory magnetic coupling, and giant magnetoresistance [1–4]. In the two-dimensional (2D) geometry, the fundamental magnetic properties of thin film nanostructures are known to differ dramatically from those of the bulk, while they may also be influenced by interactions with the supporting substrate [1,4]. This influence can occur through a variety of possible mechanisms, including elastic strain, magnetic interface anisotropy, substrate-induced stabilization of unique film structures, intermixing, and exchange biasing. Besides the need to understand how these mechanisms operate in diverse systems, it would also be desirable to harness substrate interactions to control thin film magnetism in a systematic way. This capability to control thin film magnetism could be useful for engineering magnetic devices in the future.

In this paper, we have explored the influence of ordered surface alloy substrates on the magnetic properties of ultrathin Fe films. The formation and properties of 2D alloys at crystal surfaces have attracted broad interest [5–32]. Surface alloys form when atoms that are deposited on the surface of a dissimilar material have sufficient thermal energy to overcome the activation barrier to exchange with surface atoms. This will occur if the presence of deposited atoms within or below the surface layer is energetically favored. The energetic and kinetic requirements for the formation of surface alloys are met in a significant number of adsorbate-substrate systems. The stability of surface alloys has also received particular attention because they are known to form even between many elements that are immiscible in bulk [17–32]. Whether for reasons of bulk immiscibility, energetics of the surface alloy configuration, or even kinetic limitations to the formation of more deeply penetrated alloys, alloying is very frequently confined to the topmost atomic layer. Practical interest in surface alloys as new materials has been motivated by the fact that their electronic structure and properties can differ substantially from the bulk surfaces of their constituent elements. The unique properties of surface alloys have been studied largely in connection with chemisorption and catalytic behavior in the past [11–18,25]. This outlook is encouraged by the prospect of tailoring properties through a careful selection of alloy constituents. Due to the frequency, ease, and the self-limiting nature of their formation, surface alloys also hold promise as substrates that could enrich thin film magnetic behavior and serve as a means for exercising control over thin film magnetism.

Our investigations focus on the magnetic properties of Fe films on the $c(2 \times 2)$ ordered alloys that are formed by Au, Ag, and Cu on the W(100) surface. These alloys are part of a larger class of noble metal-induced (Au, Ag, Cu, Pt, Pd) $c(2 \times 2)$ surface alloys that form on W(100) and Mo(100) refractory metal surfaces [21–32]. In the $c(2 \times 2)$ alloy structure, noble metal atoms substitute for surface Mo or W atoms in a checkerboard pattern, with an optimal metal coverage of 0.5 monolayer (ML). Local density approximation calculations have shown that electron depletion induced by an applied electric field can stabilize $c(2 \times 2)$ vacancy arrays on Mo(100) and W(100) surfaces [30,31]. Similar charge transfer that occurs to select metal adsorbates is believed to be sufficient for the stabilization of the vacancy array in which the metal atoms take up residence in the surface alloys [30–32]. Surface state shifts that occur during alloy formation are also believed to contribute to the stability of the surface alloys [32].

*huang.l@sustc.edu.cn
†phaltman@ust.hk

These electronic effects take place without significant bond formation between metal adsorbate and substrate atoms in the alloy structure, meaning that the alloys are not stabilized by d bonding [30,32]. The W(100) and Mo(100) surface alloys could therefore be interesting substrates for magnetic films because relevant aspects of electronic structure that affect magnetic properties through hybridization of electronic states at the interface, namely d bands at the Fermi level, differ significantly between the noble and refractory metals.

The growth and magnetic properties of Fe films on the W(100) surface have been studied theoretically and experimentally in the past [33–48]. In this paper, we make a comparative experimental and theoretical study of Fe films on the W(100) surface and W(100)-M $c(2 \times 2)$ (M = Cu, Ag, Au) surface alloy substrates. The onset of ferromagnetic order that occurs with increasing Fe film thickness at room temperature due to finite-sized scaling of the Curie temperature [49–52] is measured very accurately using spin-polarized low-energy electron microscopy (SPLEEM). The onset occurs precisely at a film thickness that the Curie temperature is equal to room temperature. It is marked by a sudden appearance and sharp increase of magnetic signal during continuous Fe deposition. This critical onset appears to be very sensitive to the influence of interfacial structure on thin film magnetism. Magnetic moments and exchange coupling constants of the magnetic ground state of idealized atomically flat films are also determined theoretically using first-principles density functional theory calculations. The key differences between these microscopic magnetic quantities in films on the clean W(100) surface and noble metal-induced surface alloys provide important insight about the nature of the interfacial interaction on surface alloy substrates. This insight guides our understanding of the trends in the onset of macroscopic magnetic ordering observed experimentally.

II. EXPERIMENTAL RESULTS

A. Experimental details

The W(100) sample was cleaned by annealing in oxygen at about 1400 K to remove carbon and flashing up to about 2200 K to remove oxygen. It was heated by electron bombardment, and its temperature was measured using a W/Re3%-W/Re25% thermocouple. The base pressure in the vacuum chamber was below 5×10^{-11} Torr. The chamber pressure rose to $\sim 2 \times 10^{-10}$ Torr during Fe, Cu, Ag, and Au deposition. Fe and Au were deposited from resistively heated evaporation sources, and Ag and Cu were deposited from electron beam heated evaporation sources.

The W(100)-M $c(2 \times 2)$ surface alloys were prepared by depositing Cu, Ag, or Au onto the W(100) surface at high temperature. Careful control of deposition conditions is essential for producing surface alloys with optimal long-range order reproducibly. Deposition of metal atoms to the ideal coverage of the alloy, 0.5 ML, was controlled precisely by monitoring the $c(2 \times 2)$ diffraction spot intensities during deposition. The $c(2 \times 2)$ spot integrated intensities exhibit a distinct peak during deposition that occurs at the ideal metal atom coverage when deposition is carried out in the appropriate temperature range. Alloy formation is inhibited at low temperature due to a kinetic limitation to exchange of deposited metal atoms for W atoms in the surface. For example, an indicative exchange barrier of 0.50 eV was determined for the formation of the Mo(100)-Ag $c(2 \times 2)$ surface alloy [28]. Alloy formation is also inhibited at very high temperature due to the thermal instability of the surface alloy. The nature of this instability has been shown to be an entropy-driven order-disorder transition via dealloying [29]. Noble metal desorption occurs at slightly higher temperature. In this paper, we employed deposition temperatures of 800 K for Au, 775 K for Ag, and 825 K for Cu that avoid kinetic limitations to alloy formation at low temperature and alloy instability issues at higher temperature. It has also been shown that disorder is built into the surface alloy during the formation process to a degree that is determined by alloy nucleation kinetics [28]. In particular, disorder is present at antiphase domain walls between alloy domains that form in registry with the two possible $c(2 \times 2)$ sublattices of the surface. The amount of the surface that is ultimately occupied by antiphase domain walls depends upon the number of alloy domains that nucleate. Therefore, the amount of localized disorder, which scales with the total domain wall length, can be effectively reduced by forming the surface alloy under conditions that produce a low alloy nucleation rate, fewer and larger domains. This can be achieved in practice by using deposition rates below about 0.1 ML/min at the chosen deposition temperatures [28]. Therefore, metal atom deposition rates in the range of 0.035–0.065 ML/min were used in this paper to minimize the amount of localized disorder that is associated with the presence of antiphase domain walls.

The veracity of the comparative study reported here depends upon the reliability of the Fe film thickness determination on different substrates. Film thickness was determined by the deposition time at known fixed deposition rate. The Fe deposition rate was calibrated before each SPLEEM experiment by monitoring LEEM image intensity variations during deposition of Fe on the W(100) surface at 500 K. At this temperature, the initial layer-by-layer growth produces periodic intensity oscillations corresponding to periodic nucleation, growth, and completion of an atomic layer [Fig. 1(a)]. Measurements were performed at an imaging energy of 8.0 eV, which is close to an out-of-phase interference condition that produces the strongest intensity oscillations. This is similar to the behavior that was observed before during the growth of Cr on the W(100) surface [53] and Fe on the Cu(100) surface [54]. The deposition rate is easily determined from the time interval between the beginning of deposition and the first intensity peak. An additional check of reproducibility was made by monitoring the LEEM image intensity during each subsequent SPLEEM measurement of the magnetic onset during Fe deposition that is described in more detail below. The intensity versus Fe thickness $I(t)$ for multiple SPLEEM growth experiments at room temperature on W(100) and W(100)-Au $c(2 \times 2)$ substrates is plotted in Figs. 1(b) and 1(c) based on the preceding source rate calibrations. The close agreement of $I(t)$ for each experiment confirms the reproducibility of the deposition rate calibrations and film thickness determinations. Similar reproducible $I(t)$ curves were observed for growth on the Ag- and Cu-induced surface alloys. The intensity variations during growth on W(100) at room temperature in Fig. 1(b)

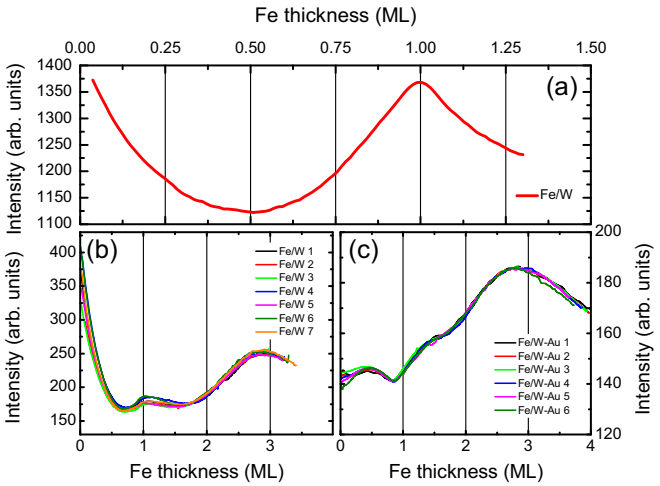

FIG. 1. LEEM image integrated intensity vs film thickness for Fe growth on (a) the W(100) surface at 500 K, (b) the W(100) surface at 300 K, and (c) the W(100)-Au $c(2 \times 2)$ surface alloy at 300 K. The imaging energy was (a) 8.0 eV, (b) and (c) 1.0 eV. The Fe deposition rate is determined from the time interval between the start of deposition and the first oscillation peak during growth on W(100) at 500 K.

differ from growth at elevated temperature in Fig. 1(a) because the former were measured at an imaging energy of 1 eV in order to enhance the SPLEEM magnetic signal. This energy is just above the threshold for total reflection in the mirror imaging mode. At this threshold imaging condition, intensity variations are also sensitive to work function changes [55].

The principles and capabilities of imaging and diffraction of LEEM and SPLEEM have been discussed previously [56,57]. Conventional LEEM imaging and diffraction are supplemented by magnetic sensitivity when a spin-polarized electron beam is used to illuminate the sample in SPLEEM. A SPLEEM image containing purely magnetic information is calculated from LEEM images that are acquired with oppositely polarized incident electron beams, called spin-up and spin-down images. The exchange asymmetry is defined as $A_{ex} = (1/P)(I_\uparrow - I_\downarrow)/(I_\uparrow + I_\downarrow)$, where $I_\uparrow$ and $I_\downarrow$ are the spin-up and spin-down intensities, and P is the magnitude of the incident beam spin polarization. The quantity $P \cdot A_{ex}$ is calculated pixel by pixel to obtain a SPLEEM image. The intensities in the SPLEEM exchange asymmetry image are proportional to the dot product of the incident beam polarization $\boldsymbol{P}$ and local sample magnetization $\boldsymbol{M}$ vectors. The azimuthal orientation of the incident beam polarization in the in-plane direction and rotation of the polarization out-of-plane are controlled by spin rotators in the illumination column of the microscope.

B. Film growth and magnetic onset

The growth and wetting behavior of Fe films on the W(100) surface have been studied previously [33–38,40–47]. It is well known that highly strained (10.4%) pseudomorphic films form at room temperature [34,35,40,41,43–45] that become increasingly rough with increasing thickness above an initial wetting layer thickness of 2 ML [41,44,45]. The 2 ML wetting layer has been shown experimentally to be thermodynamically stable [33,35,40,44–46]. Material in excess of the thermodynamically stable wetting layer thickness agglomerates into three-dimensional (3D) islands upon annealing or directly during growth at elevated temperature [33–35,38,40,41,44–46]. Films grown at room temperature exhibit in-plane magnetization [37,38,40–42,45].

The LEEM image intensity variation $I(t)$ during growth on the surface alloys at room temperature, e.g. Fig. 1(c), provides some insight about the growth mode. In particular, some similarity of the $I(t)$ that is observed during growth on the surface alloys and the clean surface suggests that the growth modes are also similar. This means that the kinetically limited growth of a rough Fe film that is known to occur on W(100) at room temperature [41,44,45] also occurs on the surface alloys.

The onset of magnetic order in Fe films on the W(100) and W(100)-M $c(2 \times 2)$ surface alloy substrates was studied by recording SPLEEM images quasicontinuously during Fe deposition at room temperature. The SPLEEM images were acquired at approximately 0.01 ML thickness intervals. Selected SPLEEM images recorded during Fe film growth on W(100) and W(100)-M $c(2 \times 2)$ are shown in Figs. 2 and 3. The incident beam polarization was oriented along the in-plane [012] direction in these experiments, midway between the high symmetry [011] and [001] directions. This assured that some component of the magnetization along either of the two most likely in-plane directions was detected. No evidence of out-of-plane magnetization was observed under any condition, in agreement with earlier work [37,38,40–42,45]. The same sample region was studied systematically in all experiments to ensure reproducibility. A LEEM image of this region on the partially Fe-covered W(100) surface is shown in Fig. 2(a). The dark features in this image are Fe islands on terraces and atomic steps decorated with Fe. This region is characterized by large terraces in the middle of the image and step bunches at the top and bottom of the image.

Magnetic ordering is suppressed in thin films due to finite size effects [49–52]. The Curie temperature T_c is suppressed below room temperature in very thin films and increases gradually towards the bulk value with increasing film thickness. The onset of ordering during film growth occurs precisely at a film thickness that T_c is equal to the deposition temperature, i.e. room temperature in the experiments reported here. It is marked by the sudden appearance of magnetic asymmetry signal in our investigations (Figs. 2–4). A sharp rise of signal strength that follows the onset reflects the further scaling of T_c with thickness beyond the onset thickness. The magnetic signal is first detected in the step-bunched regions at the top and bottom of the SPLEEM image during Fe deposition on W(100) [Fig. 2(b)]. The onset of magnetic order occurs at a slightly larger film thickness, ~0.1 ML, in the flat terrace regions at the center of the image. Magnetic domains exhibit a morphology that is reproducibly influenced by the presence of step bunches. The earlier onset in the step-bunched regions indicates that T_c is higher in these areas than on the flat terrace region. Although a step-induced enhancement of T_c was not detected in earlier experiments that looked explicitly for such an effect in Fe/W(100) [42], its presence in our experiments is irrefutable. However, we also note that the difference between the onset thicknesses in flat and stepped regions that

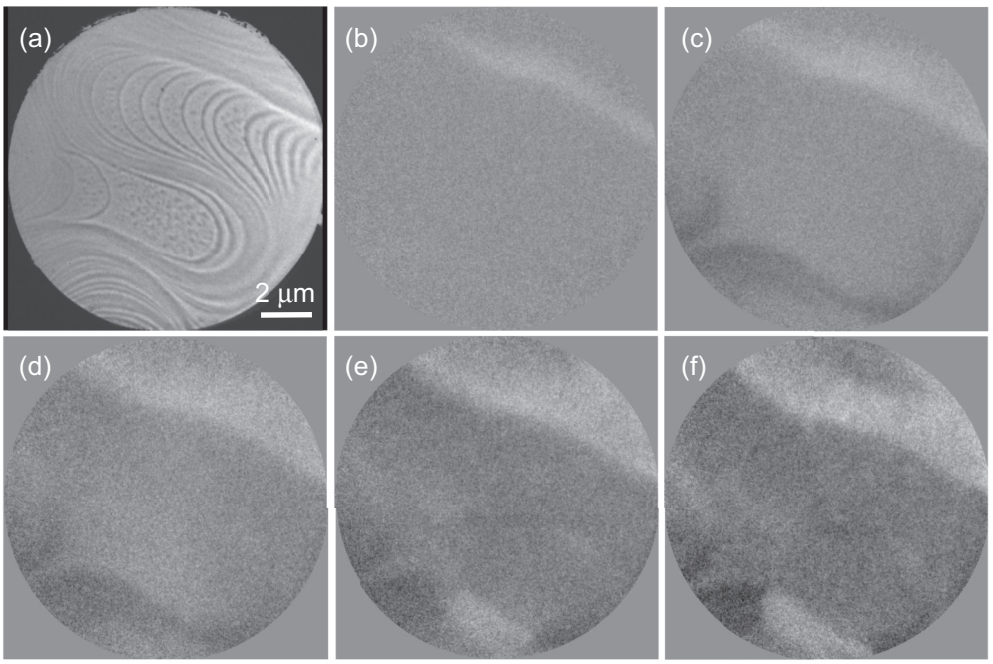

FIG. 2. (a) LEEM image of the sample area on the W(100) surface that was studied in all experiments. (b)–(f) SPLEEM magnetic asymmetry images acquired during Fe film growth on W(100) at 300 K. Film thicknesses are (b) 2.78 ML (onset in upper step bunch region), (c) 2.83 ML (onset in lower step bunch region), (d) 2.90 (onset on flat terraces), (e) 3.00 ML, and (f) 3.50 ML. The imaging energy is 1.0 eV, and the image field of view is 13 μm.

were detected was only ∼0.1 ML. This small difference is less than the thickness increment in the earlier experiments. Therefore, the small influence of steps on magnetic ordering may have easily been overlooked before. Nevertheless, in order to exclude the extrinsic effect of the substrate step-bunch morphology as much as possible in our comparative study of the magnetic onset, we confined our investigations to the initially flat terrace region at the middle of the image.

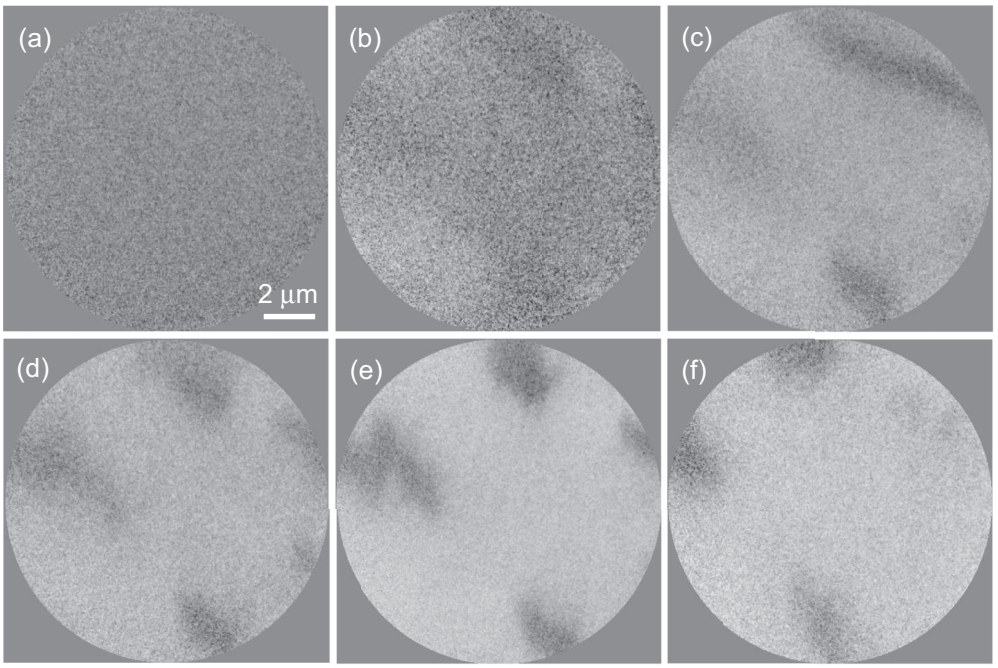

FIG. 3. SPLEEM magnetic asymmetry images acquired during Fe film growth on (a)–(d) the W(100)-Au $c(2 \times 2)$, (e) W(100)-Ag $c(2 \times 2)$, and (f) W(100)-Cu $c(2 \times 2)$ surface alloys at 300 K. Film thicknesses are (a) 2.90 ML, (b) 3.12 ML (onset), (c) 3.20 ML, (d) 3.72 ML, (e) 3.36 ML, and (f) 3.49 ML. The imaging energy is 1.0 eV, and the image field of view is 13 μm.

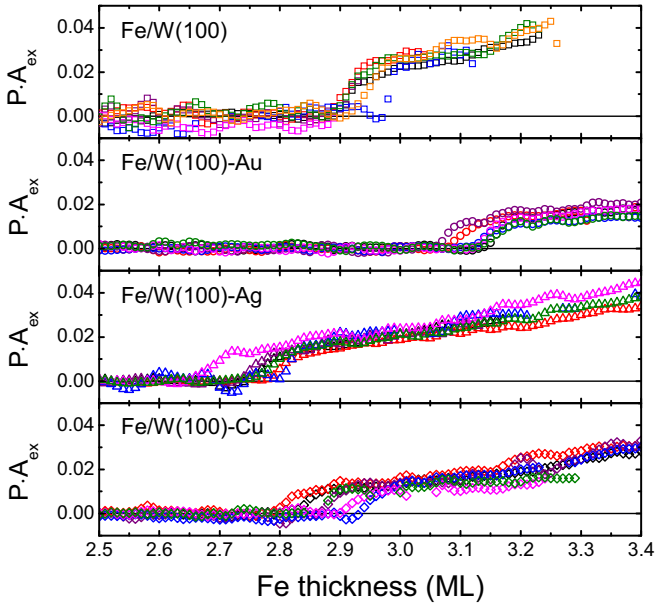

FIG. 4. Variation of magnetic asymmetry with film thickness during multiple Fe deposition experiments on the clean W(100) surface (□), and Au- (◯), Ag- (△), and Cu- (◇) induced surface alloy substrates at 300 K.

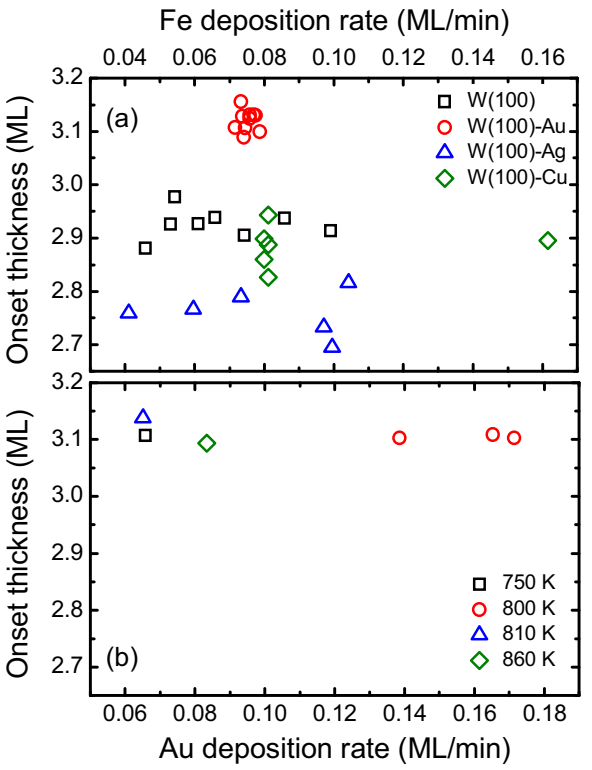

FIG. 5. (a) The magnetic onsets determined at 300 K in multiple Fe deposition experiments on the clean W(100) surface (□) and W(100)-M $c(2 \times 2)$ surface alloys [M = Au (◯), Ag (△), Cu (◇)] are plotted with respect to Fe deposition rate. (b) The magnetic onsets determined at 300 K on the W(100)-Au $c(2 \times 2)$ surface alloy are plotted with respect to Au deposition rate used to prepare the surface alloy at 750 K (□), 800 K (◯), 810 K (△), and 860 K (◇).

The evolution of the magnetic domain morphologies during Fe deposition and their overall appearances on the Au-induced alloy [Figs. 3(a)–3(d)] and Ag- and Cu-induced surface alloys [Figs. 3(e) and 3(f), respectively] were remarkably similar to each other. Interestingly, the magnetic onset did not occur earlier in the step-bunched regions compared to the initially flat terrace region on the surface alloys. It occurred more or less uniformly across the image field of view. Magnetic domains on the surface alloys also have blurrier edges than the domain boundaries that were observed in Fe/W(100), and the domain morphologies do not seem to exhibit any obvious relationship with the initial step-bunch morphology [Figs. 3(d)–3(f)].

The magnetic onset was determined precisely by measuring the exchange asymmetry quantitatively in SPLEEM images as a function of nominal Fe film thickness. The exchange asymmetry was integrated over a large area in the flat terrace region of the substrate. Plots of the integrated exchange asymmetry are shown in a narrow thickness range around the onsets for each experiment in Fig. 4. The asymmetry is zero for paramagnetic films before the onset of magnetic order. The sudden appearance and sharp rise of asymmetry that follows shortly afterwards occurs with very high reproducibility in multiple experiments that were performed on all substrates. Identifying the onset as the first nonzero data point that exceeds the noise level observed for the paramagnetic film, we determine the onset thickness on the W(100) surface to be 2.93 ± 0.03 ML, where the uncertainty represents the standard deviation of the seven experiments shown. This is consistent with previous observations of the onset in films between 2–3 ML thickness grown at room temperature on W(100) [40,41,45], although the onset in our experiments was about 0.5 ML higher. The onsets are likewise determined to be 3.12 ± 0.02 ML on the Au-induced surface alloy, 2.76 ± 0.04 ML on the Ag-induced surface alloy, and 2.89 ± 0.04 ML on the Cu-induced surface alloy. Furthermore, Fig. 5(a) demonstrates that the onsets are independent of the Fe deposition rate. We have also tested if the onset depends upon the alloy growth conditions prior to Fe deposition, thereby whether it is affected by disorder that is introduced during alloy formation [28]. Results are shown in Fig. 5(b) for the onset on Au-induced alloys formed using different Au deposition rates ranging from 0.065 to 0.17 ML/min and temperatures ranging from 750 to 860 K. The small variation of onset in this set of experiments is within the scatter for the onset on the Au-induced alloy formed using our standard conditions, ∼0.065 ML/min at 800 K [Figs. 4 and 5(a)]. Therefore, the onset of magnetic order does not appear to depend critically on the alloy formation condition.

C. Effect of metal overlayers on Fe/W(100) magnetism

An issue that arises in the use of surface alloys as substrates for magnetic films is whether the alloy is stable at the buried interface. The thermodynamic stability of the alloy will depend upon the relative surface free energies of the substrate and film surfaces. Intermixing of the alloy-inducing metal species in the Fe film, or complete segregation to the top of the growing film in the extreme case, may occur if the buried surface alloy is not stable. The prevalence for intermixing will also depend upon the kinetics of the intermixing process and the bulk solubility

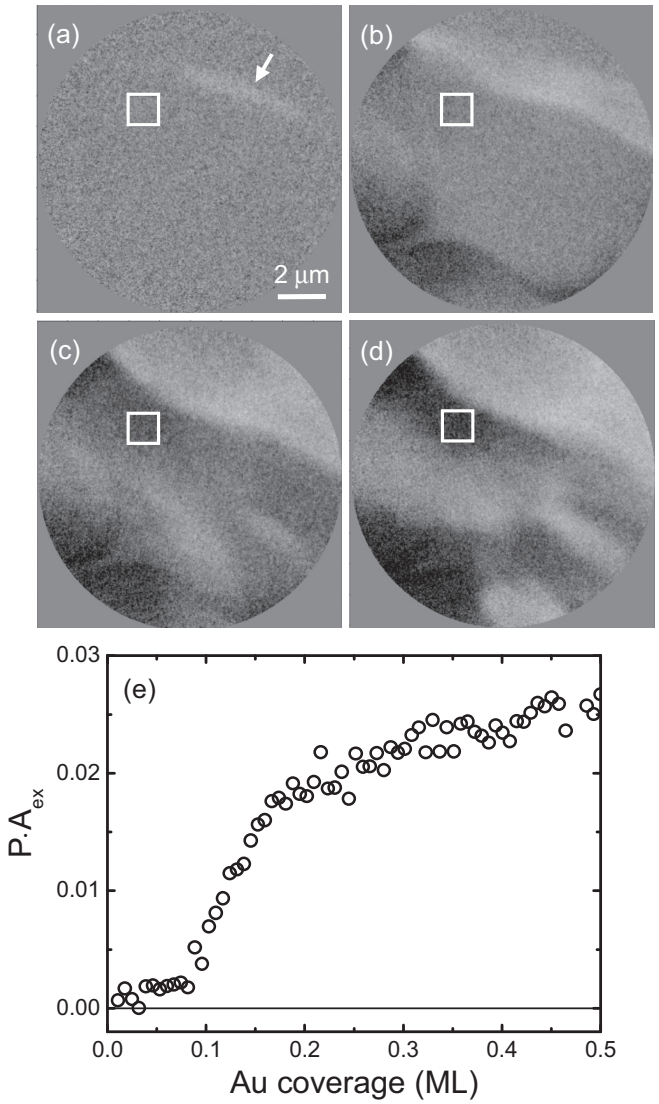

FIG. 6. SPLEEM magnetic asymmetry images acquired during Au deposition on an 2.83 ML Fe film on the W(100) surface that exhibits weak magnetic ordering initially in (a) at step bunches (arrow). Au coverages are (a) 0 ML, (b) 0.1 ML, (c) 0.2 ML, and (d) 0.5 ML. The imaging energy is 1.0 eV, and the image field of view is 13 μm. (e) Variation of magnetic asymmetry with increasing Au coverage measured in the white box indicated in the images.

of the metal in the film. Although intermixing or segregation do not occur when Fe films are grown on refractory metal substrates, noble metal surfaces show a tendency to intermix with Fe during film growth, more so for Au than for Cu and even less so for Ag [54,58–61]. A floating Au layer has even been observed during Fe growth on the Au(100) surface in the temperature range 300–530 K [58–60]. Consequently, similar tendencies on the surface alloys could likewise lead to dealloying, intermixing, and even segregation of the noble metal to the top of the growing Fe film.

We have explored the implications of intermixing empirically for the extreme case of complete surface segregation. This was done by looking at how a Au overlayer affects the magnetic onset of a Fe/W(100) film. The energetics and kinetics of segregation are also treated theoretically in Sec. III, and further discussion of this topic is presented in Sec. IV. The experiments were carried out by depositing Fe on the clean W(100) surface at room temperature until just prior to the magnetic onset. The Fe film thickness was controlled by the calibrated deposition rate, and deposition was stopped when weak magnetic contrast was just discernible in SPLEEM images in the step-bunched region at the upper part of the image, while the remainder of the film remained paramagnetic [Fig. 6(a)]. Au was subsequently deposited on top of the nearly magnetic Fe film. The onset of magnetic order that is induced by Au deposition on the initially nearly magnetic Fe film shown in Fig. 6 is obvious. The onset occurs in the flat terrace region after deposition of roughly 0.1 ML of Au [Fig. 6(b)]. This Au coverage corresponds roughly to the onset difference in Fe films without Au decoration between the stepped and flat terrace regions on the clean W(100) surface (c.f. Fig. 2). The asymmetry signal rises rapidly during additional Au deposition and saturates slowly above a Au coverage of 0.2 ML. This measurement shows qualitatively that a Au overlayer enhances ordering and raises T_c in Fe/W(100) films.

III. THEORETICAL RESULTS

A. Methods and models

All first-principles calculations were performed using the projector augmented wave (PAW) method [62,63] as implemented in the Vienna *Ab initio* Simulation Package (VASP) [64,65]. The exchange-correlation interactions were described by the generalized-gradient approximation (GGA) with the Perdew-Burke-Ernzerhof (PBE) functional [66]. An energy cutoff of 400 eV was used for the plane wave basis expansion. A 15 × 15 × 1 Monkhorst-Pack mesh was used to sample the Brillouin zone. The W(100) and W(100)-M substrates were modeled by a 9-layer slab with a $c(2 \times 2)$ surface unit cell. Pseudomorphic Fe overlayers were put on both sides of the slab. The vacuum space was set to be 12 Å in the direction normal to the surface, which is large enough to eliminate spurious image interactions. The in-plane lattice constant was fixed to the W bulk value, determined in our calculations to be 3.172 Å. All atomic coordinates were fully relaxed using the conjugate gradient method until the force acting on each atom was less than 0.01 eV/Å. The climbing image nudged elastic band (CI-NEB) method [67] was employed to investigate the intermixing and segregation of the noble metal atoms on the surface alloy substrates. A $2 \times 1 \times 1$ supercell was constructed, and a $5 \times 10 \times 1$ Monkhorst-Pack k-point mesh was used for the CI-NEB calculations.

To calculate the interatomic exchange interactions, we map the total energy of the spin system onto a classical Heisenberg Hamiltonian

$$H_{\text{eff}} = -\frac{1}{2}\sum_{i \neq j} J_{ij} \boldsymbol{s}_i \cdot \boldsymbol{s}_j, \tag{1}$$

where J_{ij} is the exchange interaction constant between two Fe atoms, and $\boldsymbol{s}_i(\boldsymbol{s}_j)$ is the unit vector pointing in the direction of the local magnetic moment at site i (j). The mapping can be done in many available schemes. The most straightforward method consists of total energy calculations

for a set of collinear magnetic structures obtained by reversing the directions of some magnetic moments and fitting them to Eq. (1) [68,69]. The second is the frozen-magnon approach, in which the exchange interaction constants are obtained by a Fourier transformation of the energy spectra of the spin-spiral waves [69–71]. This approach is successful in describing the long-range exchange interactions, but at the same time very time consuming. In this paper, we adopted the first method due to its computational efficiency. For films with 2 (3) ML Fe overlayers, self-consistent total energy calculations were performed for all the 6 (20) possible nonequivalent collinear magnetic structures, and the exchange constant J_{ij} was then determined by a least-squares fitting. Only the nearest and next-nearest neighbors exchange interactions were taken into account, which is sufficient for our qualitative discussion.

B. Magnetic ground state, magnetic moments, and heats of formation

Although bulk body-centered-cubic (bcc) Fe has a collinear spin configuration, Fe adopts a noncollinear configuration in artificially stabilized face-centered-cubic (fcc) structures [72]. Evidence of noncollinear spins in Fe/W(110) at the spin reorientation transition between in-plane collinear configurations has also been reported [73]. Collinear spin configurations were examined in earlier theoretical investigations of Fe/W(100) films [39,47,48]. Likewise, we limit the scope of our initial theoretical investigations of Fe films on the W(100)-M $c(2 \times 2)$ surface alloys and comparative investigations of Fe/W(100) to collinear magnetism.

Calculations of total energy were performed for all the possible nonequivalent collinear magnetic structures, including ferromagnetic (FM), intralayer antiferromagnetic (AFM), interlayer-AFM, and more complex spin configurations. Intralayer-AFM coupling refers to the case that nearest neighbor moments within each atomic layer are aligned antiparallel to one another. Interlayer-AFM coupling refers to the case that moments within an atomic layer are aligned parallel to one another but antiparallel to moments in adjacent atomic layers. The calculated total energies for these three configurations are shown in Table I. The other more complex spin configurations were found to have higher energy than the ground state and so are not listed. Our calculations indicate that the ground state of 1 ML Fe is AFM and that 2 and 3 ML Fe films are FM on W(100). These results agree with earlier theoretical predictions for 1 and 2 ML Fe films [39,47]. They are also consistent with experimental observations for all thicknesses [36–38,40–47]. The magnetic ground state of 1 ML Fe on the Au-induced surface alloy is likewise determined to be AFM, but it is somewhat surprisingly predicted to be FM on the Cu- and Ag-induced surface alloys. Ferromagnetic ground states are also determined for 2 and 3 ML Fe films on all surface alloys, similar to Fe/W(100).

TABLE I. Total energy (in meV) per Fe atom of different spin configurations on W(100) and W(100)-M $c(2 \times 2)$, M = Cu, Ag, Au. All energies shown are relative to the ground state.

	FM	Intralayer-AFM	Interlayer-AFM
1Fe/W(100)	131.2	0	—
2Fe/W(100)	0	51.3	128.9
3Fe/W(100)	0	140.4	185.6
1Fe/W(100)-Au $c(2 \times 2)$	17.0	0	—
2Fe/W(100)-Au $c(2 \times 2)$	0	191.4	325.4
3Fe/W(100)-Au $c(2 \times 2)$	0	129.5	242.5
1Fe/W(100)-Ag $c(2 \times 2)$	0	37.1	—
2Fe/W(100)-Ag $c(2 \times 2)$	0	195.8	334.0
3Fe/W(100)-Ag $c(2 \times 2)$	0	142.9	237.3
1Fe/W(100)-Cu $c(2 \times 2)$	0	28.9	—
2Fe/W(100)-Cu $c(2 \times 2)$	0	175.5	284.2
3Fe/W(100)-Cu $c(2 \times 2)$	0	147.4	219.8

The heat of formation per atom was calculated from the total energies using the formula

$$E_{\text{form}} = \tfrac{1}{2}\left[\tfrac{1}{2}(E_{\text{slab+overlayer}} - E_{\text{slab}} - 4E_{\text{bulk}})\right], \qquad (2)$$

where $E_{\text{slab+overlayer}}$ is the total energy of the slab covered on both sides by 2D pseudomorphic Fe overlayers. Here, E_{slab} is the energy of the slab without the overlayer, and E_{bulk} is the energy of one Fe atom in the bulk environment. For the n ML Fe film, the slab is the bare W(100) surface or surface alloy covered by an $n-1$ ML Fe film. Therefore, this formula calculates the heat of formation for the addition of a single layer. There is a factor of four because each added (over)layer on either side of the slab contains two Fe atoms. The two factors of $1/2$ account for the presence of two atoms per cell in each of the added overlayers on the two surfaces of the slab. The spin configuration with the lowest heat of formation is the magnetic ground state for each film thickness. Since this definition of E_{form} is an incremental change associated with the addition of one atomic Fe layer, it informs us about the growth mode in thermal equilibrium. If E_{form} is negative, then the added layer is thermodynamically stable, and it will wet the underlying bare substrate or previously stable underlying Fe layer. If it is positive, then the added layer will cluster into 3D islands on top of the substrate or previously stable layer.

Calculated local magnetic moments and heats of formation of the magnetic ground states are shown in Table II. We find that the magnetic moments in Fe films are generally larger than the bulk Fe moment ($2.2\,\mu_B$). Their values at the surface layer of the thickest (3 ML) films on all substrates ($\sim 3\,\mu_B$) approach the theoretically predicted enhanced values for freestanding (100) ($3.2\,\mu_B$) [39] and (110) ($3.3\,\mu_B$) [74] MLs. Compared to these enhanced surface moments, magnetic moments are suppressed in the two layers that are in closer contact with all substrates. Moments determined here for 2 ML Fe/W(100) are similar to early work [39] and in very close agreement with more recently reported theoretical values [48]. Taking the commonly enhanced moments at the 3 ML film surfaces as a reference, we find that the suppression of moments at the interface is stronger on the W(100) surface than on the surface alloys. Small moments are also induced in the top substrate layer. The moments induced by 2 and 3 ML FM Fe films are generally larger on the W(100) surface than on W atoms in the surface alloys. The induced moments on W are coupled antiferromagnetically to the FM Fe films. The larger induced moments on W at the W(100) surface correlate with the stronger suppression of moments in the Fe film on this substrate. Very small moments are also induced in the noble metals that reside in the surface alloys. These marginal induced

TABLE II. Magnetic moments and heats of formation for Fe films in the magnetic ground states identified in Table I. *M*/W1 is the first substrate layer. **Boldface** indicates induced moments on the noble metals (*M*).

	Magnetic moment (μ_B)				
	Fe3	Fe2	Fe1	*M*/W1	Heat of formation (eV)
1Fe/W(100)			2.49/−2.49	0.00/−0.00	−0.75
2Fe/W(100)		2.79	1.92	−0.29	0.15
3Fe/W(100)	2.96	2.53	2.03	−0.28	0.11
1Fe/W(100)-Au $c(2\times2)$			2.87/−2.87	**0.00**/0.00	0.64
2Fe/W(100)-Au $c(2\times2)$		2.85/2.96	2.55	**0.03**/−0.16	−0.02
3Fe/W(100)-Au $c(2\times2)$	2.99	2.62/2.59	2.67	**0.06**/−0.16	0.18
1Fe/W(100)-Ag $c(2\times2)$			2.92	**0.05**/−0.19	0.76
2Fe/W(100)-Ag $c(2\times2)$		2.85/2.96	2.54	**0.01**/−0.16	−0.05
3Fe/W(100)-Ag $c(2\times2)$	2.99	2.62/2.59	2.65	**0.04**/−0.20	0.19
1Fe/W(100)-Cu $c(2\times2)$			2.74	**0.07**/−0.24	0.37
2Fe/W(100)-Cu $c(2\times2)$		2.86/2.95	2.46	**0.03**/−0.17	−0.03
3Fe/W(100)-Cu $c(2\times2)$	2.97	2.56/2.61	2.52	**0.07**/−0.23	0.18

moments couple ferromagnetically with the FM films. The moments that are induced by 1 ML FM Fe films on the surface alloys formed by Cu and Ag are similar to moments induced by thicker Fe films on these substrates. The 1 ML AFM Fe films on W(100) and the Au-induced alloy are notably less effective at inducing moments in the substrate.

The heats of formation (Table II) indicate that 1 ML Fe/W(100) in the AFM ground state will wet the surface. However, FM 2 and 3 ML films are predicted to be thermodynamically unstable. Our calculated heat of formation for 1 ML AFM (2 ML FM) is more negative (positive) than reported previously [48]. However, note that the ground state of 1 ML Fe/W(100) was assumed to be FM in the earlier work. The corresponding heat of formation that we calculated for FM 1 ML Fe/W(100) is −0.62 eV/atom, which is nearly the same as the value, −0.57 eV/atom, that was determined earlier [48]. Fe films up to 2 ML thick have been shown experimentally to be thermodynamically stable [33,35,40,44–46]. This empirical observation suggests a small margin of error in the theoretical treatment and that 2 ML films must really be marginally stable. There are two possible reasons for this discrepancy. One is that the energies of 1 and 2 ML Fe/W(100) were taken to be their AFM/FM ground state energies in our calculations. However, the films are paramagnetic under the experimental condition at room temperature. The second reason relates to the chemical potential of Fe atoms, which was assumed to be the energy of bulk bcc Fe. This should always be smaller than the actual value of the chemical potential. The positive heat of formation determined for 3 ML/W(100) agrees with experimental observations that this thickness exceeds the thermodynamically stable wetting layer thickness [33,35,40,44–46]. However, despite the positive heat of formation, smooth metastable films thicker than 2 ML can be grown at intermediate temperature, 400–500 K [44,45]. Kinetically limited growth at even lower temperature results in increasing roughness above the initial 2 ML wetting layer [41,44,45]. On the other hand, 1 ML Fe is predicted here to be unstable on all of the surface alloys on the basis of positive heats of formation. This does not preclude kinetically limited growth at room temperature in our investigations. Interestingly, the heats of formation for FM 2 ML Fe films on all three surface alloys are negative. Speculatively, this might lead to a tendency for bilayer growth under kinetically limited growth conditions at room temperature.

C. Exchange interaction, onset of magnetic order, and segregation

To further our understanding of the influence of different substrates on the critical magnetic onset thickness, exchange constants J_{ij} that characterize pairwise coupling between moments residing at different atomic sites i, j were calculated up to the next-nearest neighbor. The results for 2 and 3 ML Fe on different substrates are presented in Figs. 7(a) and 7(b), respectively. We adopt the notation that the indices $i, j = 1,2,3$ refer to the layer number relative to the interface and use the convention that positive (negative) values of J_{ij} favor FM (AFM) order. Nearest neighbor coupling constants correspond to indices $j = i + 1$; next-nearest neighbor coupling constants correspond to $j = i$ (in-plane) and $j = i + 2$ (out-of-plane). Additional superscripts a and b distinguish inequivalent nearest neighbor coupling constants that are present in the larger unit cell on the surface alloys [Fig. 7(c)]. Note that $J^a_{ij} = J^b_{ij}$ for Fe layers on the clean W(100) substrate by symmetry.

The interlayer nearest neighbor exchange constants J^a_{ij} and J^b_{ij} play a dominant role in stabilizing magnetic order in 2 ML Fe films on all substrates, as shown in Fig. 7(a). Their positive values indicate FM ground states, which are consistent with our previous predictions for all substrates. All exchange constants are enhanced (more positive/less negative) on all three noble metal-induced surface alloys compared to the clean W(100) substrate. This is expected to enhance magnetic ordering and elevate the Curie temperature T_c in films on the surface alloys. It is worth noting that the dominant nearest neighbor exchange constants, which mainly determine the T_c, exhibit the trend W(100)-Au ≈ W(100)-Ag > W(100)-Cu > clean W(100). A similar trend is also found on balance among the strongest coupling constants for 3 ML Fe films, as can be seen in Fig. 7(b). These trends suggest that the expected

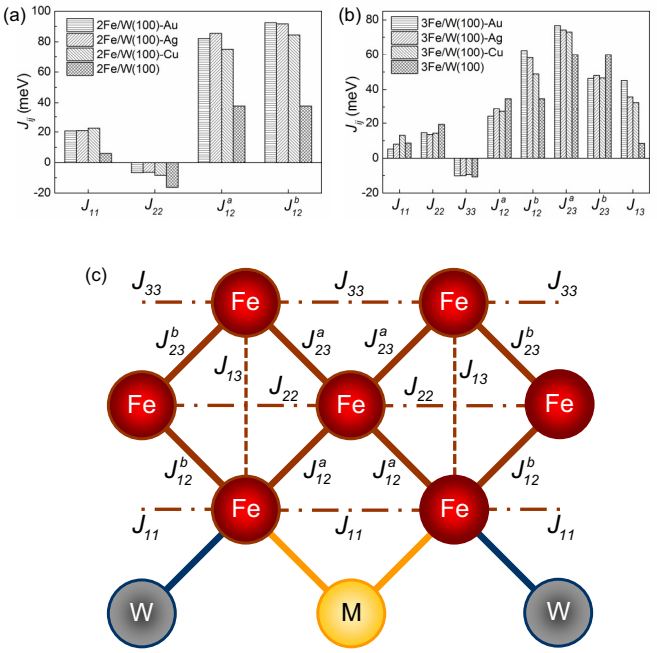

FIG. 7. Calculated exchange interactions for (a) 2 ML Fe and (b) 3 ML Fe on different substrates. (c) Exchange coupling constants projected onto a [010] plane perpendicular to the substrate surface for Fe films on W(100)-M $c(2 \times 2)$ surface alloy (replace M with W and set $J^a_{ij} = J^b_{ij}$ for Fe layers on the clean W(100) substrate). The substrate layer and second Fe layer are in the same vertical plane. Refer to the text for an explanation of the notation, $J_{ij}, J^{a,b}_{ij}$.

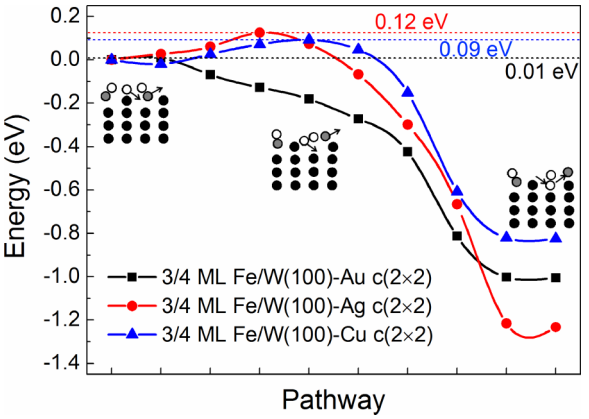

FIG. 8. Calculated energetics for Au (■), Ag (●), and Cu (▲) atom segregation from the substrate W(100)-M $c(2 \times 2)$ surface alloy layer to the 0.75 ML Fe film layer along the concerted exchange pathway shown in the projected [011] cross-sectional plane. The black, gray, and white filled balls represent W, Au/Ag/Cu, and Fe atoms, respectively.

onset thicknesses of magnetic order on the different substrates should follow the trend W(100)-Au ≈ W(100)-Ag < W(100)-Cu < clean W(100). We performed Monte Carlo simulations based on the classical Heisenberg model to confirm this expectation, considering nearest neighbor interactions only and assuming rigid spins. A supercell of 100 × 100 × 1 was used. For each temperature, the total number of Monte Carlo steps was 30 000, allowing an initial relaxation time of 5000 steps and then sampling every 50 steps. The Curie temperatures exhibit a clear trend W(100)-Au ≈ W(100)-Ag > W(100)-Cu > clean W(100) for both 2 and 3 Fe layers, which is consistent with the trends for the onset of magnetic order that we predicted based upon inspection of the coupling constants. However, the estimated values of T_c are larger than can be expected from our experimental observations, due to the inherent quantitative inaccuracy of the Monte Carlo simulations. The theoretical predictions are in qualitative agreement with the experimentally determined trend of the onset, W(100)-Ag < W(100)-Cu < clean W(100) < W(100)-Au, for the Ag-, Cu-induced surface alloys, and clean W(100) substrates, but not for the Au-induced surface alloy.

The anomalous behavior that was observed experimentally on the Au-induced surface alloy substrates may be caused by possible intermixing and segregation of Au atoms, as noted above and reported previously [58–60]. Therefore, we investigated the segregation barrier for Au, Ag, and Cu atoms during the Fe deposition process by the CI-NEB method [67]. To simulate the initial stage of growth, we constructed a 2 × 1 × 1 substrate supercell covered with partial and complete Fe MLs. We studied plausible pathways that the noble metal atoms may take in moving from the surface alloy substrate to a site on top of it. The lowest energy barriers were found for a concerted exchange process involving several Fe atoms at 0.75 ML local Fe coverage. The calculated energy landscape along the exchange pathway and a schematic drawing of the pathway are depicted in Fig. 8. The energy barriers are found to be 0.01, 0.09, and 0.12 eV for the displacement and segregation of Au, Cu, and Ag atoms, respectively. Higher barriers were found at lower Fe coverage and when the surface alloys were fully covered by Fe MLs. These results indicate that Au atoms should tend to intermix with Fe during the latter part of the growth of the first Fe ML, while Ag and Cu atoms are more likely to remain more localized in the surface alloys layer at this crucial stage of growth because of kinetic barriers to their displacement. Although Au intermixing can occur with almost no barrier when the Fe overlayer is locally close to 0.75 ML, it should be strongly kinetically suppressed at lower Fe coverage and when the Fe layer overgrows the substrate on all of the surface alloys.

For 3 ML Fe films on W(100)-M $c(2 \times 2)$ surface alloys, one Fe atom in the first (second) layer is surrounded by four (eight) nearest Fe and five (six) next-nearest Fe atoms. The segregation of a Au atom will replace such an Fe atom. Another Fe atom will also substitute into the vacancy that is left behind in the alloy layer. The substituted Fe atom is surrounded by only four nearest neighbor Fe and zero next-nearest neighbor Fe atoms. This will dramatically reduce the number of pairwise FM exchange interactions, and thus can be expected to lead to a suppression of magnetic ordering and a delay of the magnetic onset on the Au-induced surface alloy.

IV. DISCUSSION

The experimental observations reported here provide evidence that kinetically limited growth of rough Fe films occurs on the noble metal-induced W(100)-M $c(2 \times 2)$ surface alloys at room temperature, similar to the growth mode on

the clean W(100) surface [41,44,45]. This is suggested by the similar evolution of the LEEM image intensity during growth on the different substrates (cf. Fig. 1). Rough growth occurs at room temperature on the W(100) surface beyond the thermodynamically stable wetting layer thickness, determined experimentally to be 2 ML, because of limited lateral and interlayer Fe diffusion. However, unlike the stable wetting of Fe/W(100) that is predicted theoretically (Ref. [48] and Table II) and observed experimentally [33–35,38,40,41,44–46], the heats of formation determined here (Table II) indicate that 1 ML Fe should not even wet the surface alloys in thermodynamic equilibrium. Nevertheless, limited Fe diffusion should also produce continuous Fe films during growth on the surface alloys at room temperature.

We find experimentally that the onset of magnetic order during growth at room temperature varies reproducibly in films on the clean W(100) and the surface alloy substrate surfaces. The onsets occur with increasing thickness as W(100)-Ag < W(100)-Cu < clean W(100) < W(100)-Au. The theoretical results shed some light on the origin of this trend. First of all, theory indicates that the magnetic moments in the magnetic ground states for ideal flat films are suppressed at the interface on every substrate (Table II). The suppression of moments is weaker at the interface on the surface alloys than on clean W(100). Exchange coupling constants are also determined (Fig. 7) that favor FM order in 2 and 3 ML Fe films on all substrates. Furthermore, the resulting nearest neighbor and next-nearest neighbor pairwise magnetic interaction clearly strengthen ferromagnetic coupling in films on the surface alloys compared to the clean W(100) surface (Fig. 8). This should advance the magnetic onset on the surface alloys with the following expected trend: W(100)-Au $\approx$ W(100)-Ag > W(100)-Cu > clean W(100). This predicted trend is confirmed by Monte Carlo simulations of the Curie temperature. It also agrees with the experimentally observed trend except for the conspicuous discrepancy about the onset on the Au-induced alloy. The experiment and theory do not even agree qualitatively about the relative order on the clean W(100) surface and Au-induced surface alloy. This discrepancy may be due to the influences of other extrinsic factors that could suppress magnetic ordering. Several possible competing influences are discussed below.

Deviations of the Fe film from the ideal flat morphology considered theoretically could conceivably suppress magnetic ordering and delay the magnetic onset. Rough Fe film growth at room temperature on the W(100) surface is already very well known [41,44,45]. Our observations also suggest that films grow on the noble metal-induced surface alloys with increasing roughness. However, the magnetic onset on the Au-induced surface alloy did not depend on Fe deposition rate for rates that varied by up to a factor of two [Fig. 5(b)], although surface roughness may be expected to vary over this range of growth conditions. Therefore, we do not believe that this is the key factor that overrides the expected interface-induced enhancement of magnetic ordering on the Au-induced surface alloy.

Intermixing of noble metal atoms in the growing Fe film may also suppress magnetic ordering. For example, an approximate linear suppression of T_c was observed with increasing Cu concentration in bulk bcc ($100 > x > 70$) and fcc ($70 < x < 20$) Fe_xCu_{100-x} solid solutions [75]. Although the low Au concentration limit was not studied in bulk FeAu, a very similar depression of T_c was reported for Fe_xAu_{100-x} solutions in the higher Au concentration limit ($x < 40$) [76,77]. Fe growth on surfaces of bulk Cu, Ag, and Au crystals appears to exhibit different trends towards intermixing. In the most extreme case, a self-surfactant growth mode in which Au floats on the growing Fe film has been reported for the Fe/Au(100) system in the temperature range 300–530 K [58–60]. This behavior is thermodynamically driven by surface energetics and is believed to be facilitated by strain-induced enhanced solubility of Au in Fe [60]. Although intermixing during the initial interface formation in Fe/Cu(100) is also known, Cu tends to remain more localized at the interface region [54]. The presence of a floating Cu layer during Fe film growth at room temperature has been ruled out explicitly [60]. However, no intermixing was observed at the Fe/Ag(100) interface during Fe growth at room temperature and upon annealing below 200 °C [61]. Our theoretical investigations show that the energy barrier for segregation of a Au atom from the surface alloy to the first growing Fe layer nearly vanishes (0.01 eV) along a plausible low-energy concerted exchange pathway when the Au-induced alloy is locally covered by a 0.75 ML Fe film (Fig. 8). The energy barriers for Cu (0.09 eV) and Ag (0.12 eV) segregation are more substantial along similar concerted exchange pathways (Fig. 8). Interestingly, these numerical results are consistent with the trends for intermixing exhibited during Fe growth on Au, Cu, and Ag surfaces [54,58–61]. Higher energy barriers for noble metal segregation from all three surface alloys are found here at lower local Fe coverages, 0.25 and 0.5 ML, and when the alloys are covered by a complete Fe layer. These results demonstrate that segregation is feasible to some extent during growth in a limited coverage range before the completion of the first Fe ML on the Au-induced alloy. This can be expected to delay the magnetic onset. The tendencies for segregation and consequentially a delay of the magnetic onsets in Fe films on the Cu- and Ag-induced surface alloys should be lower. The more extreme scenario that Au continues to segregate to the surface of the growing Fe film appears to be unlikely. This scenario is ruled out because a Au overlayer is observed experimentally to advance the magnetic onset of an Fe/W(100) film (Fig. 6). This contradicts the delay of the magnetic onset that is observed experimentally when Fe is deposited on the Au-induced surface alloy.

The quality of long-range order within the surface alloys and the inherent roughness of the surface alloy substrates compared to the clean W(100) surface may also affect the magnetic onset. Disorder in the surface alloy arises from the presence of antiphase domain walls between alloy domains that nucleate on two different sublattices [28]. It is built into the surface alloy during the formation process to a degree that is determined by the domain nucleation kinetics. In accordance with earlier observations [28], this type of disorder should have been minimized in our measurements by the use of low metal deposition rates at sufficiently high temperature to prepare the surface alloys. We also observed that variations of the metal deposition temperature and rate that were used to prepare the surface alloy resulted in no significant variation of the onset (Fig. 5), although they should have brought about

some changes in alloy domain nucleation and ordering to some degree. Therefore, we rule out the influence surface alloy disorder in our investigations.

The surface alloys are also inherently rough. This roughness arises when deposited metal atoms exchange places with W atoms in the surface layer during their formation. The displaced W atoms then recombine with deposited metal atoms to form single atom high alloy islands on areas of the W(100) substrate that have not already been claimed by the alloy. With increasing metal coverage, alloy islands nucleate on increasingly shorter length scales [27–29]. This converts initially flat terraces on the clean surface to a predominantly two-level (up-down-up-down) surface alloy morphology that is dominated by atomic steps on a length scale that is too short to be resolved clearly with LEEM. An influence of the two-level stepped morphology of the surface alloys on magnetism is apparent in the magnetic domain morphology. Unlike magnetic domains in Fe/W(100) that clearly correlate with the step-bunch morphology on the substrate (Fig. 2), the domain morphology on the surface alloys exhibits a much weaker or no such correlation (Fig. 3). Furthermore, the earlier magnetic onset that is observed at step bunches on W(100) [Fig. 2(b)] is also absent on the surface alloys. Interestingly, the domain structures present in Fe films on the different surface alloys are remarkably similar, besides being notably different from films on the clean substrate. We are inclined to attribute this similarity among films on the surface alloys to the similarity of the surface alloy morphologies. The domain walls in films on all of the surface alloys are also very diffuse. This signals the presence of a weak in-plane magnetic anisotropy.

Considering the enhancement of magnetic order that we observe at step bunches on the clean W(100) surface (Fig. 2), one may also be inclined to attribute the early magnetic onset on the Cu- and Ag-induced surface alloys to the inherently stepped surface alloy morphology. However, there is a fundamental difference between the stepped morphology of the surface alloy substrates and the step-bunch morphology of the W(100) surface. Steps on the surface alloy alternate up and down in every azimuthal direction, whereas closely spaced and azimuthally oriented steps in a step bunch all descend or rise in the same direction. Substrate steps are known to induce an in-plane anisotropy perpendicular to steps in Fe/W(100) [38,42]. If this is also true on the surface alloys, then the presence of steps on short length scales with all azimuthal orientations on the surface alloys should cause a local magnetic frustration. This may either suppress long-range magnetic ordering, or it could induce nanodomains with different magnetization orientations on such a short length scale initially that they are not easily detected with SPLEEM due to limited spatial resolution. The origin of the enhanced magnetic order at step bunches in Fe/W(100) is itself not clear. It could be due to an intrinsic effect on magnetic moments and coupling or merely the result of a slightly larger Fe film thickness at step bunches. The variation of alloy growth conditions discussed above in the context of alloy disorder could also be expected to induce changes in the rough surface alloy morphology. Therefore, the absence of any significant change of the magnetic onset with the variation of the alloy growth condition [Fig. 5(b)] argues against a role of the surface alloy morphology. A careful comparison between the morphologies of the different surface alloys and appropriate theoretical investigations may provide more clues about the impact of the rough surface alloy morphology on thin film magnetism.

An additional intrinsic factor to consider is the possible role of the in-plane magnetic anisotropy in determining the magnetic onset. Experimentally, we find that the magnetization is oriented along the in-plane [110] direction at the onset of magnetic order during growth on the W(100) substrate at room temperature, in agreement with earlier reports [44,45]. The initial orientation at the magnetic onset on the surface alloys rather is along the in-plane [100] direction [78]. Despite the difference between the clean and surface alloy substrates in this respect being very significant, the scale of the magnetic anisotropy energetics that controls the in-plane orientation direction is very small. In particular, it is considerably smaller than the exchange coupling energies that play a dominant role in determining the onset thickness and Curie temperature. Therefore, magnetic anisotropy should not play a significant role in the phenomena reported here.

Finally, we note that the exchange coupling strengths that are determined theoretically here are distinctly thickness dependent on both the W(100) and surface alloy substrates (Fig. 7). The significance of this effect is that it may have an impact on the finite size scaling of T_c when the film thickness is changed. In other words, the observed thickness-dependent ordering manifests the combined influences of the intrinsic finite size effect and the thickness-dependent coupling strength. It was earlier conjectured that inhomogeneous strains caused by steps and other heterogeneities at the interface can cause deviations from intrinsic finite size scaling laws in the very thin film limit, i.e. below 5 ML [51]. Our results suggest that even fundamental thickness-dependent moments and exchange coupling within films that have an ideal flat interfacial boundary may in fact come into play in the very thin film regime.

V. CONCLUSION

We have investigated the influence of ordered surface alloy substrates on the magnetic properties of ultrathin Fe films. Spin-polarized low-energy electron microscopy and first principles density function theory calculations were used to study complementary aspects of growth, thermal stability, intermixing, magnetic ordering, magnetic ground state and magnetic moments, and pairwise exchange interactions of Fe thin films on the clean W(100) surface and W(100)-M $c(2 \times 2)$ (M = Cu, Ag, Au) surface alloy substrates. Although Fe is predicted not to wet the surface alloy substrates in thermodynamic equilibrium, kinetically limited growth of rough films occurs at room temperature, similar to the growth mode of Fe on W(100). Antiferromagnetic ground states are predicted for 1 ML Fe on W(100) and the Au-induced surface alloy substrate. Ferromagnetic ground states are predicted for 1 ML Fe on the Ag- and Cu-induced surface alloy substrates and for thicker films on all substrates. These theoretical results for Fe/W(100) agree with previous theoretical predictions and experimental observations. The onset of ferromagnetic order that occurs with increasing film thickness at room temperature due to finite-sized scaling of the Curie temperature is found

experimentally to vary in films on the W(100) surface and the surface alloy substrates. It is reproducibly advanced on the Ag-induced surface alloys, marginally advanced on the Cu-induced surface alloy, and delayed on the Au-induced surface alloy compared to the onset on the W(100) surface. Theory predicts that magnetic moments are suppressed at all interfaces, but this effect is less pronounced on the surface alloys. Exchange coupling strengths that favor ferromagnetic order in 2 and 3 ML films are also determined theoretically that are similarly enhanced on the surface alloys and predict the magnetic onset trend W(100)-Au $\approx$ W(100)-Ag $<$ W(100)-Cu $<$ W(100). This trend is only in partial agreement with experimental observations: W(100)-Ag $<$ W(100)-Cu $<$ W(100) $<$ W(100)-Au. The variance between experiment and theory may be due to competing factors arising from deviations from the ideal flat film geometry considered theoretically that could suppress ordering. Although film surface roughness and disorder built into the surface alloys during their formation are two such possible factors, we provide experimental evidence that these may be less important than other factors. Intermixing of noble metals in the Fe film and the intrinsic two-level roughness of the surface alloy substrate morphology are considered to be more important. A plausible concerted exchange pathway with low-energy barrier was identified by theoretical calculation at local Fe coverage of 0.75 ML that may set the trends for intermixing among the different surface alloys. Although Au displacement from the alloy layer can occur by this mechanism with almost no barrier during the latter part of growth of the first Fe ML, finite barriers are determined for Ag and Cu segregation by this mechanism. More substantial barriers are found at lower Fe coverage and after overgrowth by an Fe ML. This may account for experimental trends for the onset of magnetic order among the alloys. Spectroscopic or other measurements sensitive to intermixing may help to identify its presence during the initial interface formation. The use of different Fe film growth conditions or methods, e.g. low temperature or pulsed laser deposition, may also help to diminish intermixing. Improvements in the alloy formation process that lead to smoother surface alloy substrate morphology, if this can really be achieved, may hold a key to exposing the intrinsic effect of the flat surface alloy interface on magnetism. Despite the possible influences of extrinsic effects, the results presented here suggest that the use of the broad class of ordered surface alloys as alternative substrates may offer greater opportunities for manipulating thin film magnetism. This encourages search of similar effects on magnetic ordering and other macroscopic magnetic properties, e.g. magnetization direction, among films on other ordered surface alloys.

ACKNOWLEDGMENTS

We gratefully acknowledge funding from the Hong Kong Research Grants Council under Grant No. 600110 and from the NSFC under Grant No. 11404160, and Shenzhen Key Laboratory of Thermoelectric Materials under Grant No. ZDSYS20141118160434 51.

[1] F. J. Himpsel, J. E. Ortega, G. J. Mankey, and R. F. Willis, Adv. Phys. **47**, 511 (1998).
[2] I. K. Schuller, MRS Bulletin **29**, 642 (2004).
[3] I. R. McFadyen, E. E. Fullerton, and M. J. Carey, MRS Bulletin **31**, 379 (2006).
[4] C. A. F. Vaz, J. A. C. Bland, and G. Lauhoff, Rept. Prog. Phys. **71**, 056501 (2008).
[5] U. Bardi, Rept. Prog. Phys. **57**, 939 (1994).
[6] J. A. Rodriguez, Surf. Sci. Rept. **24**, 223 (1996).
[7] *The Chemical Physics of Solid Surfaces: Vol. 10, Surface Alloys and Alloy Surfaces*, edited by D. P. Woodruff (Elsevier, Amsterdam, 2002).
[8] J. G. Chen, C. A. Menning, and M. B. Zellner, Surf. Sci. Rept. **63**, 201 (2008).
[9] M. Wuttig, Y. Gauthier, and S. Blügel, Phys. Rev. Lett. **70**, 3619 (1993).
[10] A. Mikkelsen, M. Borg, J. H. Petersen, J. N. Andersen, and D. L. Adams, Phys. Rev. Lett. **87**, 096102 (2001).
[11] S. H. Lu, J. Yao, L. Zhu, G. L. Liu, F. Q. Liu, and S. C. Wu, Phys. Rev. B **45**, 6142 (1992).
[12] J. Breitbach, D. Franke, G. Hamm, C. Becker, and K. Wandelt, Surf. Sci. **507–510**, 18 (2002).
[13] T. Pelzer, M. Grüne, and K. Wandelt, Prog. Surf. Sci. **74**, 57 (2003).
[14] S. Hsieh, T. Matsumoto, M. Batzill, and B. E. Koel, Phys. Rev. B **68**, 205417 (2003).
[15] M. Chen, D. Kumar, C.-W. Yi, and D. W. Goodman, Science **310**, 291 (2005).
[16] C.-S. Ho, S. Banerjee, M. Batzill, D. E. Beck, and B. E. Koel, Surf. Sci. **603**, 1161 (2009).
[17] E. K. Vestergaard, R. T. Vang, J. Knudsen, T. M. Pedersen, T. An, E. Lægsgaard, I. Stensgaard, B. Hammer, and F. Besenbacher, Phys. Rev. Lett. **95**, 126101 (2005).
[18] F. Besenbacher, I. Chorkendorff, B. S. Clausen, B. Hammer, A. M. Molenbroek, J. K. Nørskov, and I. Stensgaard, Science **279**, 1913 (1998).
[19] S. Oppo, V. Fiorentini, and M. Scheffler, Phys. Rev. Lett. **71**, 2437 (1993).
[20] J. Tersoff, Phys. Rev. Lett. **74**, 434 (1995).
[21] E. Bauer, H. Poppa, G. Todd, and F. Bonczek, J. Appl. Phys. **45**, 5164 (1974).
[22] G. A. Attard and D. A. King, Surf. Sci. **188**, 589 (1987).
[23] G. A. Attard and D. A. King, Surf. Sci. **222**, 351 (1989).
[24] G. A. Attard and D. A. King, Surf. Sci. **222**, 360 (1989).
[25] G. A. Attard and D. A. King, Surf. Sci. **223**, 1 (1989).
[26] P. Hu, A. Wander, L. M. de la Garza, M. P. Bessent, and D. A. King, Surf. Sci. **286**, L542 (1993).
[27] D. Wu, W. K. Lau, Z. Q. He, Y. J. Feng, M. S. Altman, and C. T. Chan, Phys. Rev. B **62**, 8366 (2000).
[28] K. L. Man, Y. J. Feng, and M. S. Altman, Phys. Rev. B **74**, 085420 (2006).
[29] K. L. Man, Y. J. Feng, C. T. Chan, and M. S. Altman, Surf. Sci. **601**, L95 (2007).
[30] D. Singh and H. Krakauer, Surf. Sci. **216**, 303 (1989).
[31] J. G. Che, Z. Z. Zhu, and C. T. Chan, Phys. Rev. Lett. **82**, 3292 (1999).

[32] X. K. Shu, P. Jiang, and J. G. Che, Surf. Sci. **545**, 199 (2003).
[33] T. M. Gardiner, Thin Solid Films **105**, 213 (1983).
[34] X. L. Zhou, C. Yoon, and J. M. White, Surf. Sci. **203**, 53 (1988).
[35] P. J. Berlowitz, J. W. He, and D. W. Goodman, Surf. Sci. **231**, 315 (1990).
[36] R. L. Fink, G. A. Mulhollan, A. B. Andrews, J. L. Erskine, and G. K. Walters, J. Appl. Phys. **69**, 4986 (1991).
[37] G. A. Mulhollan, R. L. Fink, J. L. Erskine, and G. K. Walters, Phys. Rev. B **43**, 13645 (1991).
[38] J. Chen and J. L. Erskine, Phys. Rev. Lett. **68**, 1212 (1992).
[39] R. Wu and A. J. Freeman, Phys. Rev. B **45**, 7532(R) (1992).
[40] H. J. Elmers and J. Hauschild, Surf. Sci. **320**, 134 (1994).
[41] T. L. Jones and D. Venus, Surf. Sci. **302**, 126 (1994).
[42] H. J. Choi, R. K. Kawakami, E. J. Escorcia-Aparicio, Z. Q. Qiu, J. Pearson, J. S. Jiang, D. Li, R. M. Osgood III, and S. D. Bader, J. Appl. Phys. **85**, 4958 (1999).
[43] A. Enders, D. Sander, and J. Kirschner, J. Appl. Phys. **85**, 5279 (1999).
[44] W. Wulfhekel, F. Zavaliche, F. Porrati, H. P. Oepen, and J. Kirschner, Europhys. Lett. **49**, 651 (2000).
[45] W. Wulfhekel, F. Zavaliche, R. Hertel, S. Bodea, G. Steierl, G. Liu, J. Kirschner, and H. P. Oepen, Phys. Rev. B **68**, 144416 (2003).
[46] A. Yamasaki, W. Wulfhekel, R. Hertel, S. Suga, and J. Kirschner, Phys. Rev. Lett. **91**, 127201 (2003).
[47] A. Kubetzka, P. Ferriani, M. Bode, S. Heinze, G. Bihlmayer, K. von Bergmann, O. Pietzsch, S. Blügel, and R. Wiesendanger, Phys. Rev. Lett. **94**, 087204 (2005).
[48] S. F. Huang, R. S. Chang, T. C. Leung, and C. T. Chan, Phys. Rev. B **72**, 075433 (2005).
[49] G. A. T. Allan, Phys. Rev. B **1**, 352 (1970).
[50] C. Domb, J. Phys. A **6**, 1296 (1973).
[51] M. Farle, K. Baberschke, U. Stetter, A. Aspelmeier, and F. Gerhardter, Phys. Rev. B **47**, 11571(R) (1993).
[52] U. Gradmann, in *Handbook of Magnetic Materials*, edited by K. H. J. Buschow (North-Holland, Amsterdam, 1993), Vol. 7.
[53] K. L. Man, Q.Guo, and M. S. Altman, Surf. Sci. **600**, 1060 (2006).
[54] K. L. Man, W. L. Ling, S. Y. Paik, H. Poppa, M. S. Altman, and Z. Q. Qiu, Phys. Rev. B **65**, 024409 (2001).
[55] C. M. Yim, K. L. Man, X. Xiao, and M. S. Altman, Phys. Rev. B **78**, 155439 (2008).
[56] E. Bauer, *Surface Microscopy with Low Energy Electrons* (Springer, New York, 2014).
[57] M. S. Altman, J. Phys.: Condens. Matter **22**, 084017 (2010).
[58] S. D. Bader and E. R. Moog, J. Appl. Phys. **61**, 3729 (1987).
[59] F. J. Himpsel, Phys. Rev. B **44**, 5966(R) (1991).
[60] C. J. Pastor, C. Limones, J. J. Hinarejos, J. M. García, R. Miranda, J. Gómez-Goñi, J. E. Ortega, and H. D. Abruña, Surf. Sci. **364**, L505 (1996).
[61] S. De Rossi and F. Ciccacci, Surf. Sci., **307–309**, Part A, 496 (1994).
[62] P. E. Blöchl, Phys. Rev. B **50**, 17953 (1994).
[63] G. Kresse and D. Joubert, Phys. Rev. B **59**, 1758 (1999).
[64] G. Kresse and J. Furthmüller, Comput. Mater. Sci. **6**, 15 (1996).
[65] G. Kresse and J. Furthmüller, Phys. Rev. B **54**, 11169 (1996).
[66] J. P. Perdew, K. Burke, and M. Ernzerhof, Phys. Rev. Lett. **77**, 3865 (1996).
[67] G. Henkelman, B. P. Uberuaga, and H. Jónsson, J. Chem. Phys. **113**, 9901 (2000).
[68] P. Ferriani, I. Turek, S. Heinze, G. Bihlmayer, and S. Blügel, Phys. Rev. Lett. **99**, 187203 (2007).
[69] L. M. Sandratskii, R. Singer, and E. Şaşıoğlu, Phys. Rev. B **76**, 184406 (2007).
[70] J. C. Tung and G. Y. Guo, Phys. Rev. B **83**, 144403 (2011).
[71] M. Ležaić, P. Mavropoulos, G. Bihlmayer, and S. Blügel, Phys. Rev. B **88**, 134403 (2013).
[72] Y. Tsunoda, J. Phys.: Condens. Matter **1**, 10427 (1989).
[73] T. Ślęzak, M. Ślęzak, M. Zając, K. Freindl, A. Kozioł-Rachwał, K. Matlak, N. Spiridis, D. Wilgocka-Ślęzak, E. Partyka-Jankowska, M. Rennhofer, A. I. Chumakov, S. Stankov, R. Rüffer, and J. Korecki, Phys. Rev. Lett. **105**, 027206 (2010).
[74] X. Qian and W. Hübner, Phys. Rev. B **60**, 16192 (1999).
[75] C. L. Chien, S. H. Liou, D. Kofalt, W. Yu, T. Egami, T. J. Watson, and T. R. McGuire, Phys. Rev. B **33**, 3247 (1986).
[76] U. Gonser, R. W. Grant, C. J. Meechan, A. H. Muir Jr., and H. Wiedersich, J. Appl. Phys. **36**, 2124 (1965).
[77] V. Cannella and J. A. Mydosh, Phys. Rev. B **6**, 4220 (1972).
[78] C. Ji, L. Huang, and M. S. Altman (in preparation).